AIAA 81-0301R

Detection of Clear Air Turbulence Using a Diagnostic Richardson Number Tendency Formulation

John L. Keller* and Patrick A. Haines*
University of Dayton Research Institute, Dayton, Ohio

The performance of a diagnostic Richardson number tendency (DRT) formulation in detecting areas of relative "high risk" for encountering turbulence is discussed. The results are encouraging. An index for risk-of-encounter, c, is calculated which may be considered proportional to the probability of encountering turbulence at a given time and place. Using a data base of ten days during the 1976 turbulence survey, the mean of this index at points of pilot-documented encounters, $\bar{c}_e$, was significantly (at a level of significance >99.9%) greater than that of the background sample. The operational adaptability of the DRT formulation seems particularly attractive in that the input data can be supplied by the currently operational upper-air sounding network. An index based on c could be incorporated into flight-path optimization software. The resulting long-term favorable bias in fleet fuel consumption characteristics should lead to significant savings.

Nomenclature

c = risk-of-encounter index
c_e = value of c at encounter points
c_p = specific heat at constant pressure
E = turbulent energy density (see Fig. 1)
f = Coriolis parameter
H = height of unstable shear layer (see Fig. 1)
N = number of grid points in each domain of calculation; $N=81$ for each level and $N=810$ for the statistical calculations
p = influence function term to account for Kelvin-Helmholtz wave propagation
P = pressure
r = linear distance in grid point space ($\Delta r=1$ between each grid point)
R = gas constant for dry air
Ri = Richardson number
s = standard deviation of c for 10-day "background" sample ($N=810$)
S_e = standard deviation of c_e
t = time
t_c = "student-t" parameter to determine significance of the difference of means $\bar{c}$ and $\bar{c}_e$
u = eastward component of wind
v = northward component of wind
$\vec{v}$ = horizontal wind velocity
x = eastward coordinate
y = northward coordinate
z = vertical (height) coordinate
$|\Delta\vec{v}|$ = magnitude of vertical shear
ϵ = rate of turbulent energy dissipated at the expense of the synoptic scale motion field
θ = potential temperature
κ = R/c_p
Φ = diagnostic Ri tendency defined in Eq. (1)
ω = vertical wind component = DP/Dt

Introduction

ENCOUNTERS with atmospheric turbulence remain an important and persistent problem for the aviation community. Though progress has been made in the communication of turbulence reports to pilots, both commercial and general aviation would benefit considerably by improved forecasting and monitoring of significant regions of moderate to severe turbulence.

A most troublesome type of turbulence is associated with statically stable vertical shear layers. While turbulence generated by thunderstorms can usually be avoided by steering clear of the cloud area, that imbedded within statically stable shear layers can often be cloud-free, giving rise to clear air turbulence (CAT). The commercial and military aviation communities would especially benefit from accurate quantitative monitoring and prediction of CAT. This is due to the fact that their aircraft tend to fly near the tropopause (jet stream) level where statically stable shear layers are more common. What is the motivation for developing and implementing improved turbulence detection and forecasting techniques? The reason which initially formed the basis for earlier work remains: passenger comfort and safety. However, a more contemporary motivation has been added. Pilots report that fuel consumption rates increase "perceptively" while flying in turbulent conditions. Avoiding turbulence can save money.

DRT Formulation

An index for quantitatively measuring the potential for jet stream turbulence was defined by Roach[1] using the time rate of change of the Richardson number (Ri) following the air motion. This is the so-called diagnostic Ri tendency (DRT). Ignoring small terms, it is

$$\Phi \equiv -\frac{D}{Dt}\ell nRi = 2\left|\frac{\partial\vec{v}}{\partial P}\right|^{-1}\frac{D}{Dt}\left|\frac{\partial\vec{v}}{\partial P}\right| - \left(\frac{\partial\theta}{\partial P}\right)^{-1}\frac{D}{Dt}\left(\frac{\partial\theta}{\partial P}\right) \quad (1)$$

where

$$\frac{D}{Dt} \equiv \frac{\partial}{\partial t} + \vec{v}\cdot\nabla + \omega\frac{\partial}{\partial P} \qquad \text{and} \qquad \omega = \frac{DP}{Dt}$$

Roach's application of Eq. (1) in a case study encountered problems which arose primarily owing to the method of calculating the first term on the right, the vertical wind shear tendency. This shortcoming was greatly remedied by Oard,[2] who used the thermal wind to specify the vertical shear tendency. Following the method of Haltiner and Martin,[3] the

Presented as Paper 81-0301 at the AIAA 19th Aerospace Sciences Meeting, St. Louis, Mo., Jan. 12-15, 1981; submitted March 4, 1981; revision received Feb. 19, 1982.

*Research Meteorologist, Applied Systems Analysis.

vertical wind shear tendency is expressed in terms of isotherm packing related to frontogenesis, i.e.,

$$2\left|\frac{\partial \vec{v}}{\partial P}\right|^{-1}\frac{\mathrm{D}}{\mathrm{D}t}\left|\frac{\partial \vec{v}}{\partial P}\right| = 2Rf^{-1}P^{\kappa-1}\left|\frac{\partial \vec{v}}{\partial P}\right|^{-1}(1000)^{-\kappa}$$
$$\times\left[-\frac{\partial\theta}{\partial x}\left|\nabla\theta\right|^{-1}\left(\frac{\partial\theta}{\partial x}\frac{\partial u}{\partial x}+\frac{\partial\theta}{\partial y}\frac{\partial v}{\partial x}+\frac{\partial\theta}{\partial P}\frac{\partial\omega}{\partial x}\right)-\frac{\partial\theta}{\partial y}\left|\nabla\theta\right|^{-1}\right.$$
$$\left.\times\left(\frac{\partial\theta}{\partial x}\frac{\partial u}{\partial y}+\frac{\partial\theta}{\partial y}\frac{\partial v}{\partial y}+\frac{\partial\theta}{\partial P}\frac{\partial\omega}{\partial y}\right)\right] \tag{2}$$

The second term, the static stability tendency, is expressed as

$$-\left(\frac{\partial\theta}{\partial P}\right)^{-1}\frac{\mathrm{D}}{\mathrm{D}t}\left(\frac{\partial\theta}{\partial P}\right)$$
$$=\left(\frac{\partial\theta}{\partial P}\right)^{-1}\left(\frac{\partial\theta}{\partial x}\frac{\partial u}{\partial P}+\frac{\partial\theta}{\partial y}\frac{\partial v}{\partial P}+\frac{\partial\theta}{\partial P}\frac{\partial\omega}{\partial P}\right) \tag{3}$$

The meteorological variables of u, v, and θ can be obtained more-or-less directly from the synoptic scale, upper-air network. The vertical velocity, ω, must be obtained indirectly. Since accurate values are required, the field is obtained through an iterative solution of the full balance ω equation using quasi-geostrophic ω's for the initial guess field.

Parentage of CAT at Jet Stream Altitudes

The quantity Φ derived above concerns the tendency of the Richardson number due to synoptic scale processes. The empirical evidence has established CAT at jet stream altitudes as a smaller, mesoscale phenomenon in which $Ri \rightarrow \frac{1}{4}$ locally. Clearly, the relationship needs to be reconciled.

The relationship lies in the energetical coupling between synoptic scale statically stable shear layers and the mesoscale CAT layers. CAT is a manifestation of the dissipation of the energy "locked-up" in jet streams (vertical shear layers). The mechanism by which this occurs, schematically illustrated in Fig. 1, is due to Kelvin-Helmholtz (K-H) gravity wave destabilization; a mesoscale phenomenon. From left to right, it shows the creation of larger, synoptic scale statically stable shear layers within which smaller mesoscale discontinuities can exist. These shallower layers can then absorb gravity wave energy due to cumulus convection, terrain wind interaction, or other random sources below via critical layer absorption. Amplifying K-H instabilities may then form at these levels, ultimately "breaking" to form turbulence when $Ri = \frac{1}{4}$.

Since the energy available to produce CAT owes its parentage to larger, synoptic scale processes, it is possible to obtain a measure of CAT potential without explicitly considering the K-H mechanism. The potential for this type of CAT should be related directly to the rate of turbulent energy dissipation resulting from breaking K-H waves. A measure of the rate of turbulent energy dissipated in this way at the expense of the synoptic scale was found by Roach[1] to be

$$\epsilon = \begin{cases} |\Delta\vec{v}|^2\Phi & \Phi<0 \\ 0 & \Phi\geq 0 \end{cases} \tag{4}$$

The factor $|\Delta\vec{v}|^2$ is a measure of the energy potentially available to form K-H instabilities within a vertical layer ΔP.† The diagnostic Ri tendency at the synoptic scale, Φ, helps determine the amount of this energy which can be released for this process.

†For statically stable conditions, pressure and altitude are often interchanged for computational convenience. A ΔP of 100 mb is about 1 km in altitude but this varies somewhat with height.

In practice, the value of $|\Delta\vec{v}|^2$ can be calculated by

$$|\Delta\vec{v}|^2 \simeq \left|\frac{\partial\vec{v}}{\partial p}\right|^2(\Delta P)^2 \tag{5}$$

It can be seen that perhaps a more accurate name for the turbulence associated with jet streams is Kelvin-Helmholtz turbulence rather than clear air turbulence (CAT). There is no reason that K-H instabilities and their associated turbulence need be strictly excluded from layered clouds. Such K-H instabilities and turbulence are occasionally observed in cloudy shear layers. Classical CAT is due to this phenomenon occurring in cloud-free shear layers at jet stream altitudes.

K-H Waves and the Risk of Encountering Turbulence

The rate of turbulent dissipation, ϵ, given by Eq. (4) is with respect to the synoptic scale motion field. The CAT of concern here is associated with turbulent dissipation resulting from breaking K-H waves. Observational (Gary[4]) and theoretical evidence (Haines,[5] Lindzen and Rosenthal[6]) indicates that these waves propagate horizontally in all directions away from their area of generation, usually at about the mean wind speed. The synoptic scale perturbations responsible for ϵ propagate at much slower speeds. Hence encounters with turbulence of this type should be clustered within and adjacent to concentrations of relatively large ϵ; volumes of the atmosphere which act as "source regions" for K-H instabilities.

Consistent with the conceptual considerations developed above, a risk of encounter index can be defined. At any calculation point, i,

$$(c)_i = \epsilon_i + \sum_{n=1}^{N=81} p_n \tag{6}$$

where p_n is the value of ϵ at a distant point, n, propagated to the calculation point according to

$$p_n(r) = \begin{cases} \epsilon_n/r & \epsilon>0 \\ \epsilon_n/r^2 & \epsilon=0 \end{cases} \tag{7}$$

where r is distance in grid point space. The propagation of K-H waves and imbedded turbulence away from a source region is incorporated in Eq. (7). Maintenance of these waves should be energetically less favorable where $\epsilon=0$ than where $\epsilon>0$, hence the more rapid attenuation of p. The physical basis of c suggests at least a relative measure of probability of encountering turbulence: increasing c corresponding to an increasing probability.

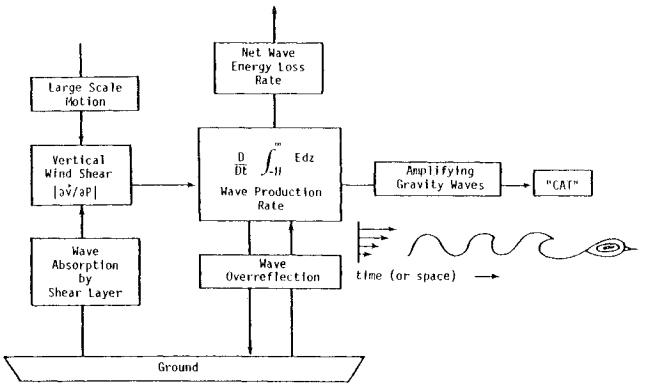

Fig. 1 CAT mechanism.

Results

The DRT technique was applied to actual National Meteorological Center (NMC) analyses derived from upper-air sounding network data. Fields of ϵ and c were calculated for 20 different observation times with $\Delta P = 100$ mb. These corresponded to ten preselected 24-h periods during which there were pilot-documented encounters with moderate or greater turbulence. The ten days selected were those selected by Dutton[7] as part of the 1976 turbulence survey by the British Central Forecast Office (CFO) in cooperation with most commercial airlines serving the European sector.

Consider Fig. 2. This figure shows the pressure heights (solid lines) and isotachs (dashed lines) for 0z March 18, 1976 at 250 mb (the z refers to Greenwich meantime). Shaded areas delineate regions of highest wind velocity. The wind direction will generally parallel the lines of constant height. How this translates into ϵ is shown in Fig. 3. Indicated are pilot encounters for a number of hours following the observation time, where turbulence was initially reported is indicated by a letter and where it ended by the head of the arrow. Note that, generally, CAT encounters tend to be clustered adjacent to maxima in ϵ. An interesting feature can be pointed out in comparing Figs. 2 and 3. The maxima in ϵ evident over the British Isles would not likely be resolved using conventional subjective CAT forecasting rules.

Figures 4-7 illustrate how the fields of ϵ relate to the risk index c. Shown are the locations of pilot CAT encounters occurring within 1 h of the observation time (1100z-1300z). By not considering the other encounters, the need for interpolating in time is eliminated.

The risk index, c, was calculated at the pressure heights (350, 300, 250, and 200 mb) characteristic of jet stream altitudes using the 12z analyses for the ten randomly selected days. The statistics in terms of sample means, $\bar{c}$, and standard deviations, s, are summarized in Table 1. The general tendency for $\bar{c}$ to increase with decreasing pressure is consistent with the climatological increase in wind shear with height. The number of individual encounters occurring during this period within an hour of 12z are shown (under e) at their respective pressure levels. There were a total of 22 CAT encounters during this period: 13 at 350 mb, 5 at 300 mb, 3 at 250 mb, and 1 at 200 mb. The risk index mean for encounters, $\bar{c}_e$, was 32.5 at 350 mb, 21.2 at 300 mb, and 88.3 at 250 mb.

Only at 350 mb are there enough encounters to speak meaningfully about the significance between the mean of the "background" sample shown in Table 1 and the encounter sample mean. Evoking the central limit theorem, a comparison of means is made using "student-t" significance levels (Panofsky[8]), where

$$t_c = \bar{c}_e - \bar{c} \Big/ \sqrt{\frac{N_e s_e^2 + N s^2}{N_e + N - 2}\left(\frac{1}{N_e} + \frac{1}{N}\right)} \qquad (8)$$

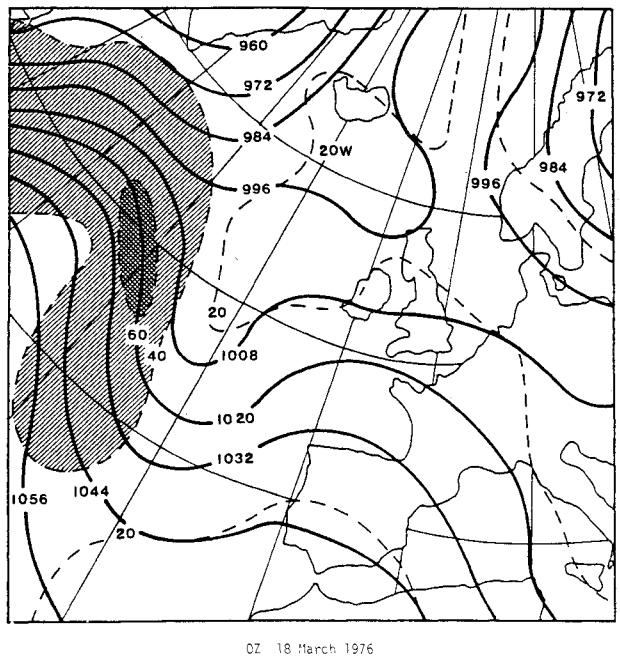

Fig. 2 Pressure heights in decameters (solid lines) and isotachs (ms^{-1}) (dashed lines) at 250 mb.

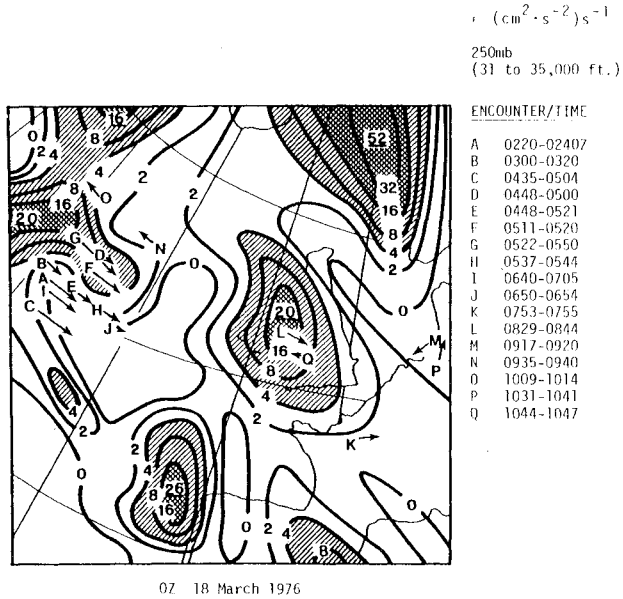

Fig. 3 Turbulent dissipation, ϵ, for the 1000-m interval centered at 250 mb and pilot encounters with moderate to severe turbulence. Maximum values of ϵ are indicated by underlining.

Table 1 Summary of CAT encounter statistics

	350 mb			300 mb			250 mb			200 mb			Totals	
Date	$\bar{c}$	s	e	$\bar{c}$	s	e	$\bar{c}$	s	e	$\bar{c}$	s	e	$\bar{c}$	e
3-09-76	13.8	10.9		13.6	12.2	1	66.9	50.7		132.8	94.2		56.8	1
3-12-76	9.8	9.9		16.9	10.6	3	73.1	59.2	2	90.1	71.5		47.5	5
3-15-76	21.7	26.6		7.2	5.2		41.1	36.5		96.7	73.1		41.7	
3-18-76	25.5	27.3	2	23.3	22.9		23.1	15.4	1	55.7	53.7	1	31.9	4
3-21-76	14.2	10.9		12.7	15.4		36.7	29.0		122.7	94.6		46.6	
3-24-76	20.5	18.6	6	12.5	7.0	1	67.3	36.5		102.2	71.8		50.6	7
3-27-76	16.3	14.8	3	7.8	5.8		50.9	36.2		120.0	115.0		48.8	3
3-30-76	11.9	14.4		11.3	17.7		40.0	34.8		103.0	84.9		41.6	
4-02-76	5.1	4.7	1	17.3	13.6		30.6	23.1		173.0	156.1		56.5	1
4-05-76	11.4	9.0	1	15.9	12.6		31.0	17.0		85.3	60.9		35.9	1
	$\bar{c}$	s	Total	$\bar{c}$	s	Total	$\bar{c}$	s	Total	$\bar{c}$	s	Total	$\bar{c}$	s
	15.0	16.3	13	13.8	13.4	5	46.1	36.3	3	108.2	92.1	1	45.8	22

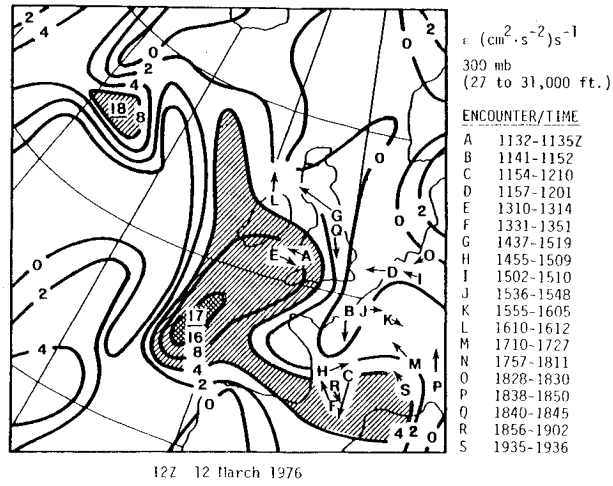

Fig. 4 Same as Fig. 3, except for map time and height indicated.

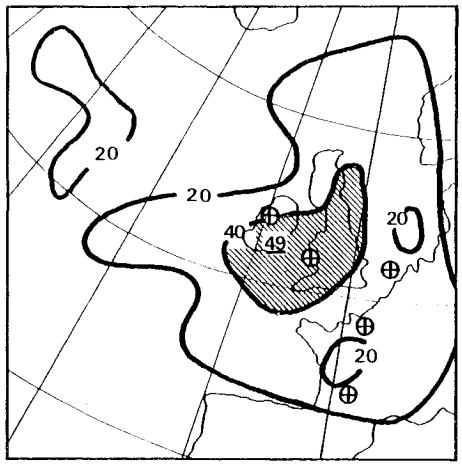

Fig. 5 Risk-of-encounter index, *c*, corresponding to Fig. 4.

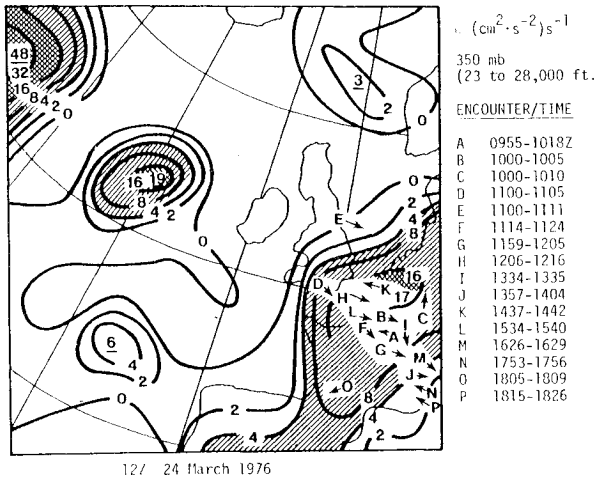

Fig. 6 Turbulent dissipation, ε, and encounters at 350 mb.

The results are shown in Table 2. For encounters at 350 mb, $t_c = 3.84$, which is a significance level of greater than 99.9%. If all encounters are used, regardless of their actual encounter level (i.e., assigned the value of c for 350 mb at their latitude and longitude), $t_c = 2.50$, which is just under the 99.0% level of significance. The values of c_e have a low probability of being a random sample from the background c. The inference which may be drawn from this is that the greater the value of c at a given point the greater the risk of encountering turbulence.

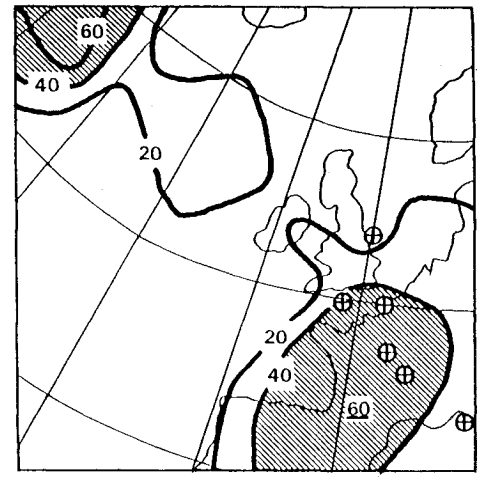

Fig. 7 Risk-of-encounter index, *c*, corresponding to Fig. 6.

Table 2 Significance of means—350 mb

Background:	$\bar{c} = 15.0$	
	$s = 16.3$	
	$N = 810$	
350-mb encounters only:	$\bar{c}_e = 32.5$	
	$s_e = 14.8$	
	$N_e = 13$	
	$t_c = 3.84$	(>99.9%)
All encounters:	$\bar{c}_e = 23.8$	
	$s_e = 16.1$	
	$N_e = 22$	
	$t_c = 2.50$	(≤99.0%)

Summary and Conclusions

Using a deterministic DRT formulation, an index may be calculated which, operationally, lends itself to a probabilistic interpretation. The physical basis of this technique concerns the energetical coupling between the synoptic scale dynamics and Kelvin-Helmholtz waves.

Further model developmental work in both software and statistical analyses are desirable. This includes a parameterization for the effects of significant terrain, an appropriate time-interpolation scheme to aid in forecasting applications, and calibration of c for each pressure level to obtain an index which more closely measures actual encounter probability. Calculations of fields 12 h apart indicate that the fields of c are fairly conservative so that a simple advective time interpolation scheme may suffice.

Pursuing the DRT technique further seems justifiable. Ultimately, fields of turbulence probabilities could be incorporated into flight-path software. Weighing this factor against the many other factors requiring consideration, an optimum flight path could be obtained. The resulting "bias" towards efficiency should result in an impressive aggregate fuel savings, even if it were to be only on the order of 1%. Finally, the technique does not require the implementation of any new observational hardware; the current upper-air network would provide the necessary observational base.

References

[1] Roach, W.T., "On the Influence of Synoptic Development on the Production of High Level Turbulence," *Quarterly Journal of the Royal Meteorological Society*, Vol. 96, 1970, pp. 413-429.

[2]Oard, M.J., "Application of a Diagnostic Richardson Number Tendency to a Case Study of CAT," *Journal of Applied Meteorology,* Vol. 13, No. 7, Oct. 1974, pp. 771-777.

[3]Haltiner, G.L. and Martin, F.L., *Dynamical and Physical Meteorology,* McGraw-Hill, New York, 1957, pp. 287-289.

[4]Gary, B.L., personal communication, JPL-NASA, 1980.

[5]Haines, P.A., "On The Intensity of Clear Air Turbulence from Detailed Wind and Temperature Observations," NASA Report in progress, 1982.

[6]Lindzen, R.S. and Rosenthal, A.J., "On the Instability of Helmholtz Velocity Profiles in Stably Stratified Fluids When a Lower Boundary is Present," *Journal of Geophysical Research,* Vol. 81, Jan. 1976, pp. 1561-1571.

[7]Dutton, M.J.O., "Performance of Conventional Operational Forecasts of Clear Air Turbulence During the 1976 Turbulence Survey," *The Meteorological Magazine,* Vol. 108, March 1979, pp. 61-76.

[8]Panofsky, H.A. and Brier, G.W., *Some Applications of Statistics to Meteorology,* The Pennsylvania State University, University Park, Pa., 1968, pp. 58-64.